Macromolecules

ARTICLE

pubs.acs.org/Macromolecules

Effects of Interfacial Interactions and Film Thickness on Nonequilibrium Hierarchical Assemblies of Block Copolymer-Based Supramolecules in Thin Films

Joseph Kao,[†] Joseph Tingsanchali,[‡] and Ting Xu*[,†,§,⊥]

[†]Department of Materials Science and Engineering, [‡]Department of Chemical Engineering, and [§]Department of Chemistry, University of California, Berkeley, Califonia 94720, United States

[⊥]Materials Sciences Division, Lawrence Berkeley National Laboratory, Berkeley, Califonia 94720, United States

ABSTRACT: The macroscopic alignment of hierarchical assemblies of block copolymer- (BCP-) based supramolecules in thin films is investigated as a function of interfacial interaction and film thickness. We specifically focus on how these two parameters affect the longevity of supramolecular morphology where BCP microdomains are oriented normal to the surface. As the film thickness increases above one equilibrium period of supramolecular assembly, hierarchical assemblies with vertically aligned BCP microdomains can be long-lived metastable state when the volume fraction of the comb block is higher than 0.5. The perpendicular-to-parallel reorientation process strongly depends on the strength of the surface field, the chemical nature of the surface, and the film thickness. The longevity of the vertically aligned assemblies can be attributed to two reasons. One is the spatial distribution of small molecules that mediate the interactions between each BCP block with the underlying substrate and the other is the comb−coil architecture of the supramolecule. These studies provide critical guidance to manipulate assemblies of supramolecules in thin films and access transient nanostructures.

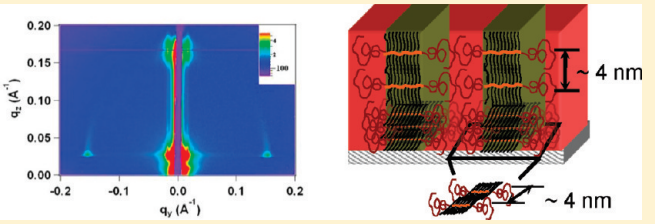

INTRODUCTION

Functional thin films with hierarchical assembly down to the molecular level are desirable to build complex scaffolds or nanodevices.[1−3] Small molecules have rich chemical functionalities and can assemble into well-defined structures at the molecular level. Block copolymer- (BCP-) based supramolecules may synergistically combine the processability and self-assembly of block copolymers with many advantages of small molecules.[4−12] Coil−comb supramolecules can be readily constructed by attaching small molecules to the polymer side chain via hydrogen bonding, electrostatic interactions or metal coordination.[5,13−16] The small molecules assemble within the microdomain and the supramolecules produced a rich library of hierarchical structures in the bulk spanning multiple length scales.[5,13,15−20] By varying the small molecules attached to the BCP, new functionalities can be incorporated at will without chemically modifying the BCPs. These supramolecules can also direct the assemblies of nanoparticles with exceptional spatial precision and generate responsive naoncomposites.[21]

In thin films, it is desirable to simultaneously control the macroscopic alignment of both the BCP microdomains and the small molecules to achieve macroscopic responses of functional small molecules.[22−32] Understanding the phase behavior of supramolecules in thin films also provides information necessary to direct the nanoparticle assemblies in thin films. For conventional coil−coil BCPs, the microdomain orientation in a thin film is mainly determined by the interfacial interactions between each component with the underlying substrate, the surface tension of each component and the incommensurability between the film thickness and the equilibrium period of the BCP morphology.[22−25,33−35] Preferential interactions of either block with the substrate will force a parallel orientation of the microdomains.[22−25,35,36] Orientation of the microdomains normal to the surface often depends on a delicate balance between the interfacial interactions of each component with the substrate and an incommensurability between the period of the BCP and the film thickness.[27]

In the case of BCP-based supramolecules, however, the assembly process is more complicated. Upon attaching the small molecules to one block of the BCP, the architecture of the supramolecules changes to a coil-comb type that forms hierarchical structures. The ordering, orientation and spatial distribution of the small molecules change the chain configuration of the comb block, the interactions between each component as well as the interfacial interactions between each component with the underlying substrate, the entropic penalty associated with deforming the comb block of the supramolecule, and potentially the phase behavior of the supramolecules in thin films. For some supramolecules, thermal annealing can only be implemented over a very narrow temperature range, due to the possible evaporation

Received: December 19, 2010
Revised: April 27, 2011
Published: May 12, 2011

of the small molecules. Thus, solvent annealing has been the method of choice to achieve supramolecular ordering in thin films.[37−42] The presence of solvent mediates the interactions between the components comprising the supramolecule and their interfacial interactions, and, therefore, must be taken into consideration. Although the solvents improve the mobility of each component, the structures obtained by solvent annealing can be in a nonequilibrium state.[40,43] Various parameters listed above will affect the local free energy minimum, thus the stability and lifetime of the nonequilibrium states.

A series of studies have been carried out to investigate the phase behavior of BCP-based supramolecules in thin films. One family of model supramolecules is constructed based on a di-BCP, polystyrene-*block*-poly(4-vinylpyridine) (PS-*b*-P4VP). 3-Pentadecylphenol (PDP) is attached to the P4VP block via hydrogen-bonding, producing the PS-*b*-P4VP(PDP)$_r$ supramolecule, where r is the stoichiometry of PDP to 4VP unit. ten Brinke et al. showed that for films of PS-*b*-P4VP(PDP)$_r$ supramolecules with thicknesses below one or two equilibrium periods, L_o, incommensurability between the film thickness and period of the assembly led to a wide range of morphologies after solvent annealing.[39,44] For thicker films, the BCP microdomains were observed to orient parallel to the surface of the film due to the preferential interfacial interactions between the comb block and the underlying oxide substrate and the lower surface tension of the comb block.[2,38,39]

With similar supramolecules, there are several reports that BCP microdomains are oriented normal to the surface after solvent annealing.[38,40−42,45−47] Subsequent removal of the small molecules produced nanoporous thin films that were then used in the fabrication of nanostructured devices.[45,48,49] We investigated the phase behavior of thin films of the same family of supramolecules, over a range of P4VP(PDP)$_r$ volume fractions, i.e. f_{comb} from 0.3−0.85.[40] The volume fraction of P4VP(PDP)$_r$ comb block can be tailored by varying either the stoichiometry of the PDP to P4VP or using BCPs with different molecular weights of the P4VP block.[2,38−40] There is a clear correlation between the fraction of comb block and the macroscopic alignment of the supramolecular assemblies. For PS-*b*-P4VP(PDP)$_r$ with f_{comb} < 0.5, the BCP microdomains oriented parallel to the surface, consistent with results observed by ten Brinke et al.[38] Upon increasing the f_{comb} > 0.5, however, the BCP microdomains oriented perpendicular to the surface and the lamellae from the P4VP(PDP)$_r$ comb block oriented parallel to the surface. This is consistent with results reported by other groups.[45−47] Experimentally, it was observed that the supramolecules undergo microphase separation during spin-casting when f_{comb} > 0.5.[40] This morphology generated during spin-casting establishes a framework within which the supramolecules order upon solvent annealing. Since there are preferential interactions between the comb block with the substrate and a lower surface tension of the comb block to segregate to the surface, thin films where the BCP microdomains are oriented normal to the surface are in a kinetically trapped state.[22,24] There have been limited studies on the stability of nonequilibrium nanostructures.[41−43,50] It is important to identify critical parameters that govern the kinetics of the reorientation process and the stability of nonequilibrium states. These studies will provide critical information to design processing conditions to manipulate assemblies of supramolecules in thin films and access transient nanostructures.

Here, we investigated the effects of interfacial interactions, film thickness and the small molecule loading on the macroscopic alignment of BCP-based supramolecules in thin films. Under solvent annealing conditions investigated here, we showed that the morphologies where BCP microdomains were oriented normal to the surface are in a kinetically trapped state. The perpendicular-to-parallel reorientation process strongly depends on the strength of the surface field, the chemical nature of the surface and the film thickness. The reorientation of the BCP microdomain occurs more rapidly for films on substrates that have strong preferential interfacial interactions with the PS coil block. Such effects are considerably reduced for films on a surface with favorable interactions with the comb block. This can be attributed to the coil-comb architecture of the supramolecule. As the film thickness increases above one equilibrium BCP period, L_o, the effects of surface fields diminish rapidly and the BCP microdomains can be macroscopically oriented normal to the surface on different substrates, regardless of the strength of the surface field. However, the underlying substrate has a strong influence on the macroscopic alignment of the lamellae of comb block within the BCP microdomains.

The supramolecular assemblies in thin films overcome the bottleneck imposed by interfacial interactions and film thickness to macroscopically align the BCP microdomains normal to the surface. Present studies investigated various energetic contributions influencing the assembly process in supramolecular thin films and identified parameters governing the stabilities of nonequilibrium states. This contribution clearly defines the processing window within which both the BCP microdomains and small molecule orientation can be manipulated. These studies are also valuable to direct hierarchical assemblies of nanoparticles in thin films.

Table 1. Characteristics of Supramolecules Used[a]

sample	$M_{n,PS}$ (g/mol)	$M_{n,P4VP}$ (g/mol)	r	f_{comb}
SP1	40 000	5600	1	0.35
SP2	40 000	5600	2.5	0.54
SP3	31 900	13 200	1	0.62
	24 000	9500	1	0.61
SP4	31 900	13 200	2	0.74
	24 000	9500	2	0.73

[a] r: molar ratio of PDP to 4VP repeat unit. f_{comb}: weight fraction of P4VP(PDP)$_r$.

EXPERIMENTAL SECTION

Materials. Diblock Copolymers. PS(40000)-*b*-P4VP(5600) (PDI = 1.09) and PS(24000)-*b*-P4VP(9500) (PDI = 1.08) were purchased from Polymer Source, Inc. PS(31,900)-*b*-P4VP(13,200) (PDI = 1.08) was synthesized in house. 3-*n*-Pentadecylphenol (95%) was purchased from Acros. Chloroform was purchased from Fisher. All chemicals were used as received.

Sample Preparation. The characteristics of all samples used in this paper are listed in Table 1. The diblock copolymer, PS-*b*-P4VP, was first dissolved in chloroform to form 1%−2% (w/v) stock solutions. The desired amount of PDP was dissolved in chloroform. The PS-*b*-P4VP solution was then added dropwise to the PDP solution, followed by stirring overnight. Thin films were prepared by spin-coating the mixed solutions onto silicon wafers or polystyrene (PS) brush modified silicon wafer at spinning speeds between 1000 and 3000 rpm. Sample thicknesses were measured using a Filmetrics F20 interferometer.

Surface Modification. To modify the silicon wafer with PS brush, 6 mg of α-hydroxyl ω-benzocyclobutene terminated polystyrene (8 wt %

BCB, M_n = 90800 g/mol, PDI = 1.41) was dissolved in 2 mL of toluene to prepare the PS brush solution. Then, the PS brush solution was spun coated onto the silicon wafer at 1500 rpm. The silicon wafer was then heated at 250 °C under N_2 flow for 20 min. The heat-treated wafer was washed with toluene 3 times at 1500 rpm. Finally, the thickness of the PS brush was measured using a Filmetrics F20 interferometer. The thickness of the PS brush was 10−15 nm. For TEM studies, ∼20 nm PS brushes were prepared on top of a NaCl plate in a similar manner.

Solvent Annealing Conditions. For solvent annealing condition one, thin films were placed together with a beaker of 40 mL of chloroform at 22.5 °C inside an inverted dish (170 mm in diameter × 90 mm in height) on top of two sheets of Texwipe. For better adhesion between the inverted dish and Texwipe, parafilm was wrapped around the rim of the dish. A weight of ∼2 kg was loaded on top of the dish. With the setting, 13 mL out of 40 mL of chloroform remained after 48 h. For solvent annealing condition two, samples were annealed for 20 min inside a 125 mL tight sealed jar with 100 μL of chloroform at 22.5 °C.

GISAXS. Grazing incidence small-angle X-ray scattering (GISAXS) measurements were made on beamline 7.3.3 in ALS at Lawrence Berkeley National Laboratory and on beamline 8-ID-E the APS at Argonne National Laboratory. X-ray wavelengths of 1.687 and 1.240 Å were used. The scattering profiles were collected on an ADSC Quantum 4u CCD detector at ALS. Line averaged intensities are reported as I vs q, where $q = (4\pi/\lambda)\sin(\theta/2)$, λ is the wavelength of incident X-rays, and θ is the scattering angle.

AFM. Atomic force microscopy (AFM) was performed either on a Digital Instruments BioScope with a Nanoscope IIIa controller or on a Molecular Imaging PicoSPM II with a PicoScan 2500. The spring constant of the cantilever was 10−130 N/m with a resonant frequency in the range of 204−497 kHz. The set point for auto tune was 2.5 V. The set-point amplitude was 90% of the free vibration value.

Transmission Electron Microscope (TEM). For TEM studies, PS-*b*-P4VP(PDP)$_r$ thin films were coated on sodium chloride (NaCl) disks in a manner similar to those on silicon substrates. To investigate the effect of interfacial interactions, cross-linked PS brush layer was prepared using a similar method to that on a silicon substrate. After solvent annealing, films were floated off the substrate onto a pool of water. Thin films were retrieved with carbon film coated copper grids and stained by exposing to iodine (I_2) vapor for 2 h to enhance the contrast. TEM images were collected on a FEI Tecnai 12 transmission electron microscope at an accelerating voltage of 120 kV.

RESULTS

Table 1 lists six PS-*b*-P4VP(PDP)$_r$ supramolecules constructed using three PS-*b*-P4VP BCPs with different stoichiometries between the PDP and 4VP repeat unit. The volume fraction of P4VP(PDP)$_r$ comb block was adjusted by varying either the volume fraction of P4VP block in the BCP or the PDP:4VP stoichiometry, r. Lamellar and cylindrical BCP morphologies were obtained by using the same BCP with different PDP:4VP ratios. SP3 and SP4 supramolecules with f_{comb} of ∼0.61 and 0.73, respectively, were constructed using two BCPs, PS(31 900)-*b*-P4VP(13 200), and PS(24 000)-*b*-P4VP(9500), that have similar volume fraction of P4VP block.

To evaluate the effects of interfacial interactions, two types of substrates were used. One is silicon substrate with a ∼2 nm native silicon oxide layer. This substrate has favorable interactions with P4VP block and was used in all of previous studies. The other type of substrate is silicon substrate modified using cross-linked PS brush, ∼10 nm in thickness. In this case, the substrate interacts favorably with the PS block and was used to investigate the effects of interfacial interactions and the supramolecular architecture on their thin film phase behavior.

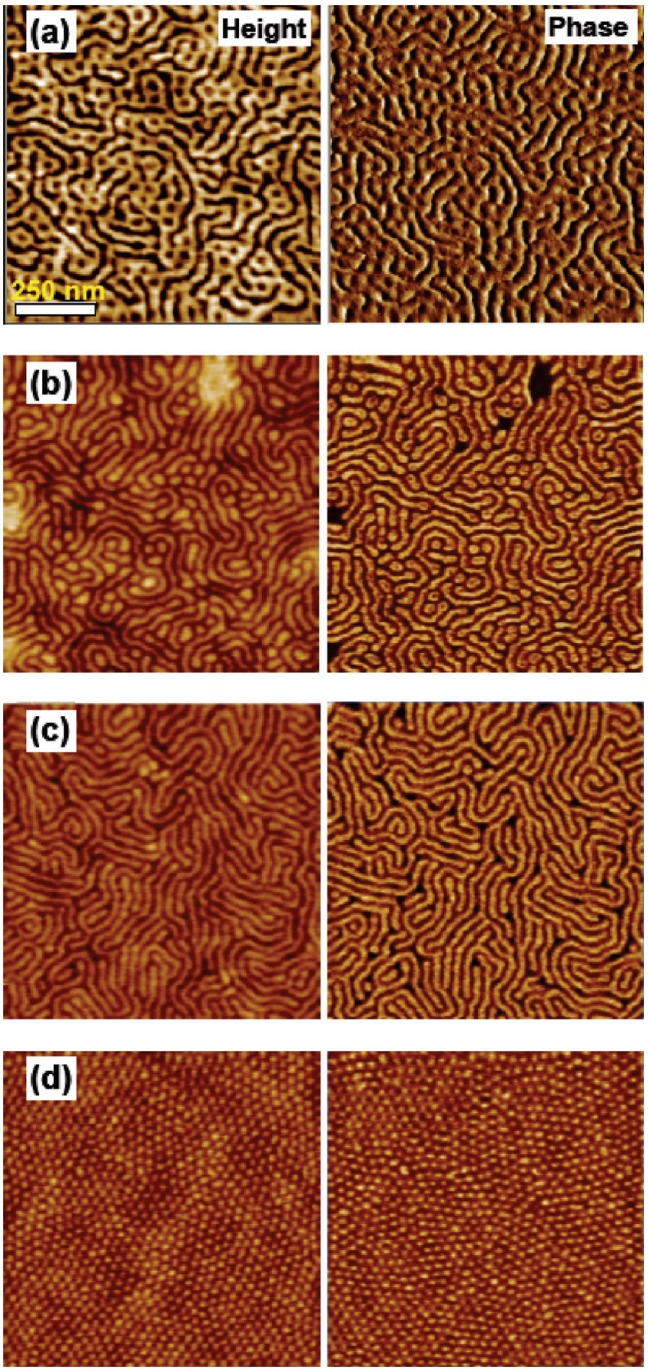

Figure 1. Morphology evolution of ∼30−40 nm thick PS-*b*-P4VP(PDP)$_r$ films on SiO_2 as f_{comb} increases. AFM height and phase images of (a) SP1, ∼30 nm in thickness, (b) SP2, ∼32 nm in thickness, (c) SP3, ∼38 nm in thickness, and (d) SP4, ∼31 nm in thickness.

Two solvent annealing conditions were used as detailed in the Experimental Section. Under solvent annealing condition one, thin films can be annealed for extended period of time (days) without observation of dewetting. This allows the supramolecular thin films to reach equilibrium states more closely. Under solvent annealing condition two, dewetting was observed after 1 h annealing. However, samples can be annealed repeatly for

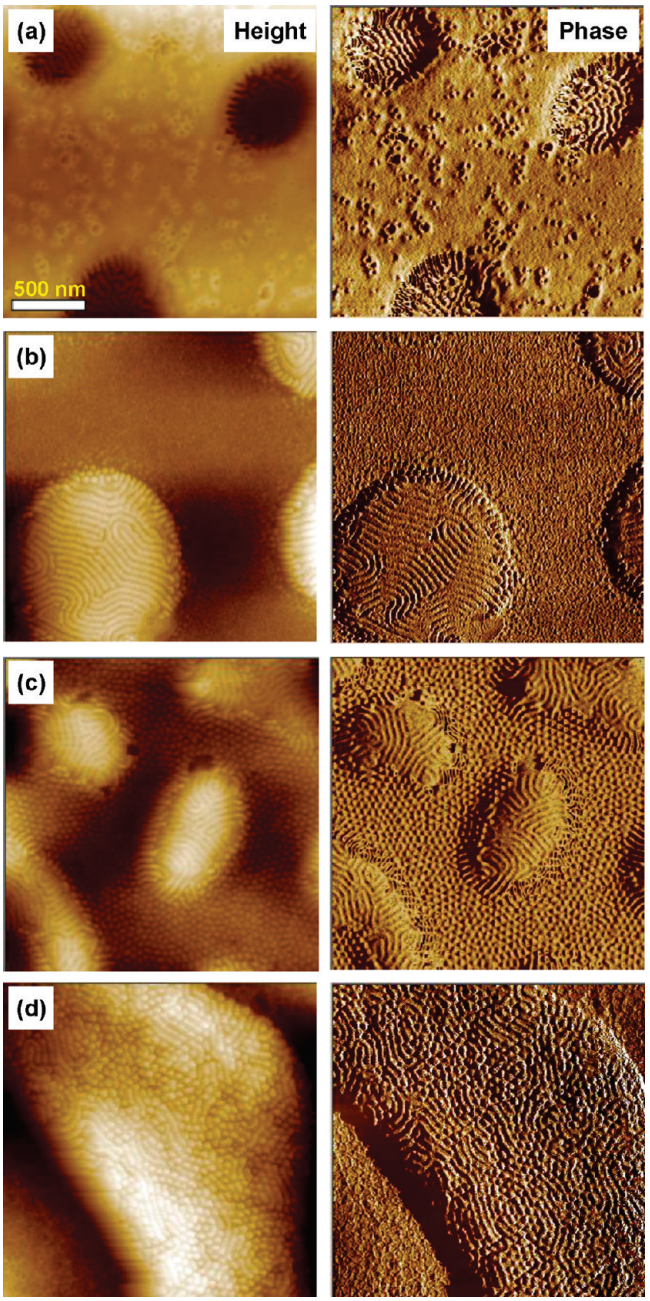

Figure 2. Morphology evolution of ~30−40 nm PS-*b*-P4VP(PDP)$_r$ films on PS brush as f_{comb} increases. AFM height and phase images of (a) SP1, ~32 nm in thickness, (b) SP2, ~46 nm in thickness, (c) SP3, ~30 nm in thickness, and (d) SP4, ~46 nm in thickness.

integral total of 20 min without dewetting. Samples were prepared at the same time under identical solvent annealing conditions. Multiple experiments have been carried out to ensure the reproducibility.

Figure 1 shows the AFM phase images of four supramolecules in thin films, ~30−40 nm in thickness, on Si substrate with native oxide layer after solvent annealing. For SP1 (f_{comb} = 0.35), the surface morphologies depend on the film thickness. A 30 nm (~0.75L_o) thin film of SP1 shows a mixture of morphologies containing features appearing to be cylinders and lamellae oriented normal to the surface (Figure 1a) after solvent annealing under condition one. For a ~40 nm (~1L_o) SP1 thin film, surface features oriented normal to the surface were not seen. The film surface was essentially flat with crack-like features on the surface, ~2 nm in depth. As f_{comb} is slightly higher than 0.5, the BCP microdomains are oriented normal to the surface in ~30 nm films of SP2, SP3 and SP4 as shown in Figure 1b-d even though the surface tension and the interfacial interactions between each component with the underlying substrate are not balanced.

SP2 and SP3 have similar f_{comb}, but different volume fraction of P4VP block and the PDP:4VP ratio. Circular donut-like features, in addition to vertical lamellae, were seen for SP2, but not for SP3. This is likely due to the inhomogeneous distribution of PDP in SP2 that has a higher PDP to 4VP ratio, where r = 2.5. For SP4, the volume fraction of P4VP(PDP)$_r$ comb block is 0.73 and a 33 nm thin film of SP4 shows hexagonally packed cylinders oriented normal to the surface (Figure 1d). Similar results were observed for thin films annealed under solvent annealing condition two. Overall, these observations are consistent with previous reports where upon increasing the volume fraction of P4VP(PDP)$_r$ comb block, f_{comb} > 0.5, the BCP microdomains can be macroscopically aligned normal to the surface.

Figure 2a−d shows the AFM images of thin films of SP1−4 on the PS-modified substrates that favorably interact with the coil block of supramolecule. The film thicknesses are between 30 and 40 nm, i.e., ~0.7−1.2L_o. With the solvent annealing condition one, islands and holes are clearly visible for all cases. Preferential interactions between the PS-modified substrate and the coil PS block lead to parallel alignment of the BCP microdomains. SP1 shows the formation of holes and SP2, SP3, and SP4 show the formation of island. Interestingly, SP3 shows a cylindrical microdomain morphology in the matrix. Since the film thickness is less than one L_o, incommensurability affects the morphologies of supramolecules in thin films and strongly depends on the film thickness.[38] This will be a subject of future study.

On the basis of the results shown in Figure 1 and 2, we conclude that the assemblies with the vertical alignment of BCP microdomains shown in Figure 1 for f_{comb} > 0.5 are in a kinetically trapped nonequilibrium state. BCP microdomains can be oriented parallel to the surface.[38] The longevity of the vertical alignment depends on the chemical nature of the substrate. Surfaces that preferentially interact with the coil block appear to lead to a faster kinetics of parallel alignment of the BCP microdomains that of surfaces with favorable interactions with the comb block.

There is a finite distance over which the surface field strongly biases the BCP microdomain alignment and morphology.[36] Effects of film thickness on the macroscopic alignment of the supramolecular assemblies were also investigated. Films with thicknesses ranging from 60 to 300 nm were prepared on both substrates. Figure 3 shows the AFM images of ~80−100 nm thin films of SP1−4. For SP1 thin films annealed under the condition one, AFM and GISAXS studies show that the BCP microdomains are oriented parallel to the surface and small lamellae from the P4VP(PDP)$_r$ comb block are oriented perpendicular to the surface. Thin films of SP1 annealed under the condition two show some features on the surface on either SiO_2 or PS-modified substrate. GISAXS indicated that the films are in a transition state to orient the BCP microdomains parallel to the surface. However, as the value of f_{comb} increases for SP2, SP3 and SP4, AFM images show that the BCP microdomains are macroscopically aligned normal to the surface (Figure 3a−f) without the formation of islands and holes. Figure 4 shows the in-plane TEM image

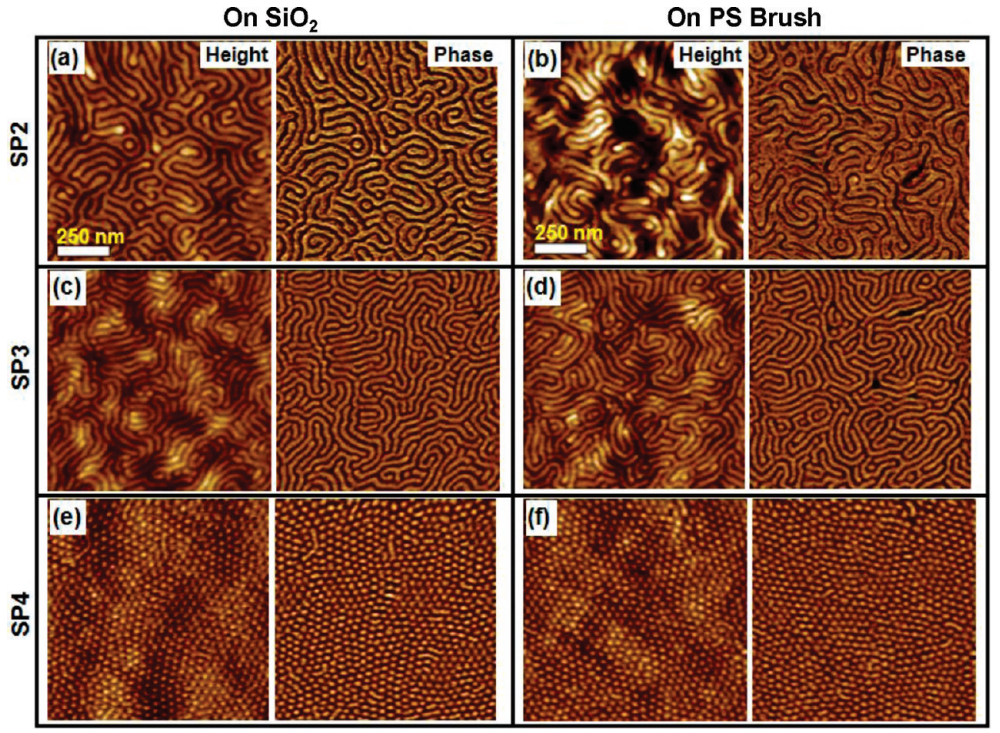

Figure 3. Morphology evolution of ~80−100 nm PS-*b*-P4VP(PDP)$_r$ films on SiO_2 and cross-linked PS brush as f_{comb} increases. AFM height and phase images of (a) SP2 on SiO_2, ~81 nm in thickness, (b) SP2 on PS, ~88 nm in thickness, (c) SP3 on SiO_2, ~86 nm in thickness, (d) SP3 on PS, ~89 nm in thickness, (e) SP4 on SiO_2, ~97 nm in thickness, and (f) SP4 on PS, ~103 nm in thickness.

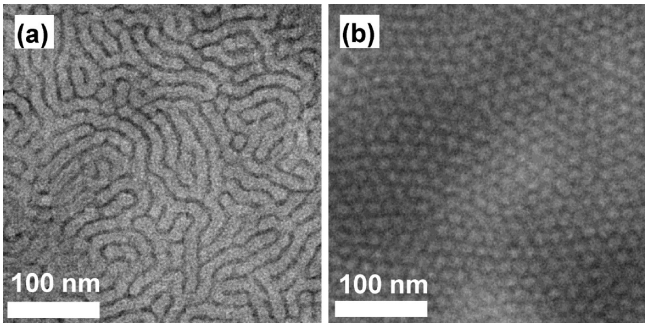

Figure 4. (a) In-plane TEM image of a ~83 nm SP3 thin film on cross-linked PS brush; (b) In-plane TEM image of a ~64 nm SP4 thin film on cross-linked PS brush. The sample has been stained with I_2 for 2 h.

of a ~83 nm thin film of SP3 and a 63 nm SP4 prepared on a ~20 nm cross-linked PS brush layer. Lamellar microdomains oriented normal to the surface throughout of film can be clearly seen. Further solvent annealing up to 72 h under the solvent annealing condition one did not lead to changes in the macroscopic alignment of supramolecular assemblies in thin films.

The hierarchical assemblies of thin films of PS-*b*-P4VP(PDP)$_r$ was studied using GISAXS. Parts a and b of Figure 5 show the GISAXS patterns of ~80−90 nm thin films of SP3 on the substrates with native silicon oxide layer and cross-linked PS brush, respectively. For both films, the GISAXS patterns are consistent with the AFM images, showing that the lamellae are macroscopically oriented normal to the surface. The q_y scans at q_z = 0.0272 Å^{-1}, show reflections corresponding to lamellar microdomains with a periodicity of 35.9 nm (q_y = 0.0175 Å^{-1}) and 36.3 nm (q_y = 0.0173 Å^{-1}) for thin films on SiO_2 and PS-modified substrates, respectively. However, the azimuthal angle dependence of the diffraction ring associated with the small lamellae of the P4VP(PDP)$_r$ comb block is clearly different.

For SP3 thin film on SiO_2 surface (Figure 5a), q_z scan at q_y = 0.0178 Å^{-1} shows a diffraction peak at q_z ~ 0.165 Å^{-1}, that corresponds to the comb block lamellae, with a period of ~3.8 nm, oriented parallel to the surface. However, for the SP3 thin film on PS-modified substrates, the diffraction peaks were also observed along the horizon. The q_y scan at q_z = 0.0272 Å^{-1} shows a diffraction peak at q_y = 0.153 Å^{-1}, originated from small lamellae, with a period of ~4.1 nm, oriented perpendicular to the surface. Similar results were seen for thin films of SP2 and SP4 on the PS-modified substrates. Thus, experimental results showed that for supramolecular thin films with thickness above $1L_o$, with the f_{comb} > 0.5, BCP microdomains can be easily oriented normal to the surfaces. Such vertical alignment can be obtained for film thickness well above $1L_o$ without applying external fields even though the interfacial interactions are not balanced. However, the macroscopic alignment of small length scale lamellae strongly depends on the interfacial interactions.

DISCUSSIONS

The incommensurability between the film thickness and the equilibrium period of supramolecule affects the macroscopic alignment and morphologies of supramolecules in thin films. However, experimentally, we did not observe dramatic differences in supramolecular assemblies for thin films of PS-*b*-P4VP(PDP)$_r$ with thicknesses above $1L_o$. This may be due to the fact that the thin films are in a nonequilibrium state. It is also likely that the presence of solvents alleviates the effects of incommensurability. To gain some basic understanding of these nonequilibrium

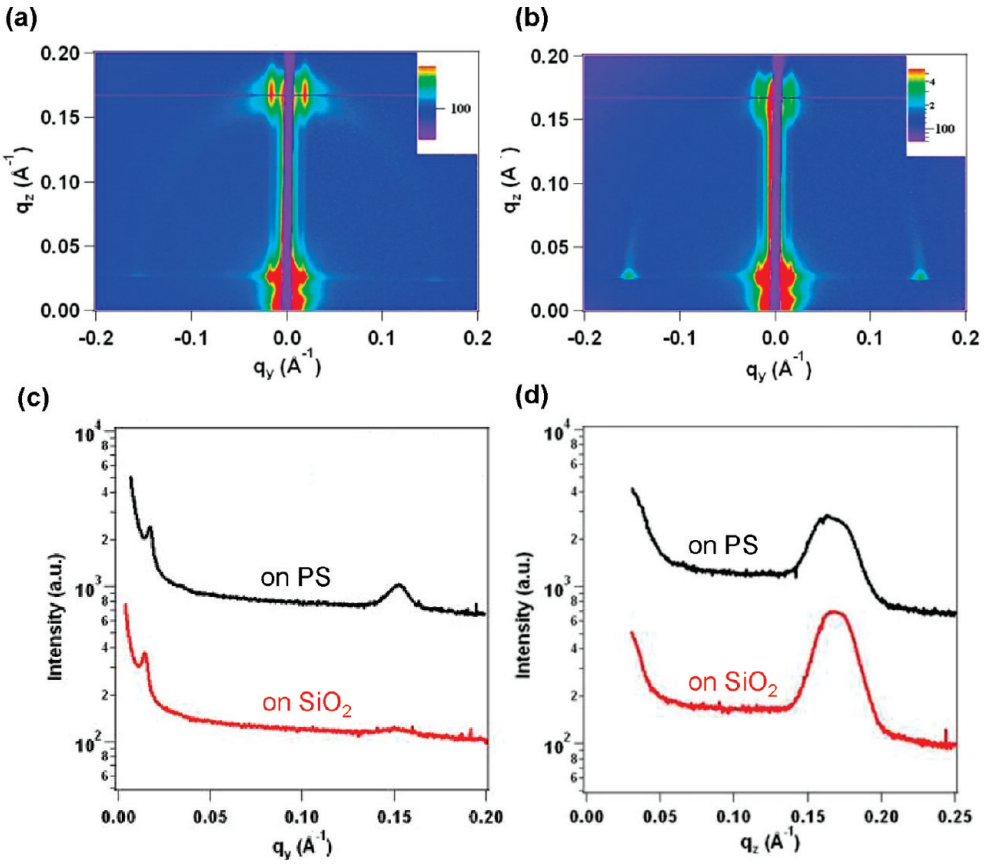

Figure 5. (a) GISAXS pattern of a ~86 nm SP3 thin film on SiO_2 at an incident angle of 0.15°. (b) GISAXS pattern of a ~89 nm SP3 thin film on cross-linked PS brush at an incident angle of 0.15°. (c) q_y scan at $q_z = 0.0277$ Å^{-1} for part a, showing the BCP lamellar microdomains with a 35.9 nm periodicity are oriented normal to the surface. q_y scan at $q_z = 0.0272$ Å^{-1} for part b, showing the lamellar microdomains with a 36.3 nm periodicity are oriented normal to the surface. The small peak at $q_y = 0.153$ Å^{-1} indicates that SP3−4 thin film has P4VP(PDP)$_r$ lamellae, 4.11 nm in period, oriented perpendicular to the surface near the PS-modified substrate. The scans are extracted from the right side of the GISAXS patterns. (d) q_z scan at $q_y = 0.0196$ Å^{-1} for part a and the q_z scan at $q_y = 0.0178$ Å^{-1} for part b, which indicate that both samples have P4VP(PDP) lamellae, ~3.8 nm in period, oriented parallel to the surface in the films.

supramolecular assemblies, we will only focus on the effects of interfacial interactions, film thickness and the volume fraction of the P4VP(PDP)$_r$ comb block. A systematic investigation on the incommensurability will be pursued in later studies.

In addition to their coil−comb architecture, the noncovalent linkage of small molecules to polymer side chain adds numerous complications to the system. The effective stoichiometry, i.e. the number of PDP attached to the P4VP block determines the interfacial interactions, χ, surface tension, architecture and chain conformation. Since the attachment is via noncovalent interactions, the effective stoichiometry depends on the boundary condition at both interfaces and the amount of solvent in the film. All of supramolecules studied here have a PDP: 4VP ratio equals to or higher than 1 and a fraction of PDPs are not hydrogen bonded to the P4VP block. Differences in the surface tension and interfacial interactions among PDP, PS, and P4PV determine the spatial distribution of PDPs at the air/supramolecule surface and substrate/supramolecule interface, which, in turn, affect the longevity of metastable states as seen in the following discussions. The chain conformation and spatial arrangements of polymer chains at both interfaces are very complicated. Furthermore, the systems investigate here are at nonequilibrium states and the resulting assemblies depend on the solvent field during spin-casting and post treatments. Here, to simplify the discussion that mainly focuses on the macroscopic alignment of BCP microdomains and lamellae of comb block, we assume homogeneous distribution of PDP along the film depth.

Using a PS-*b*-P4VP(PDP)$_r$ supramolecule that forms a lamellar-in-lamellar morphology as an example, Figure 6 schematically shows six of many possible supramolecular assemblies in thin films. They are divided into two groups, labeled with "parallel" and "perpendicular" based on the macroscopic alignment of BCP lamellae. Parts a and b of Figure 6 show the parallel alignment where the PS block and PDP have lower interfacial interactions with the substrate, respectively. Thin films of PS-*b*-P4VP(PDP)$_r$ contain alternating PS and P4VP(PDP)$_r$ lamellae oriented parallel to the surface. This is similar to symmetric coil−coil diblock copolymers. For both cases, the small lamellae of the P4VP(PDP)$_r$ comb block, with a period of ~4 nm, are oriented perpendicular to the surface.

For coil−coil symmetric BCPs, parallel lamellae were observed in thin films as long as there are preferential interactions between one block with the substrate. This is not the case for thin films of supramolecules with coil-comb architectures. Surfaces with favorable interactions with coil and comb block, respectively, may lead to different assemblies and kinetics of the assembly. When the P4VP wets the substrate, the favorable P4VP/substrate interactions pin down the P4VP block onto

dx.doi.org/10.1021/ma102857f |*Macromolecules* 2011, 44, 4392–4400

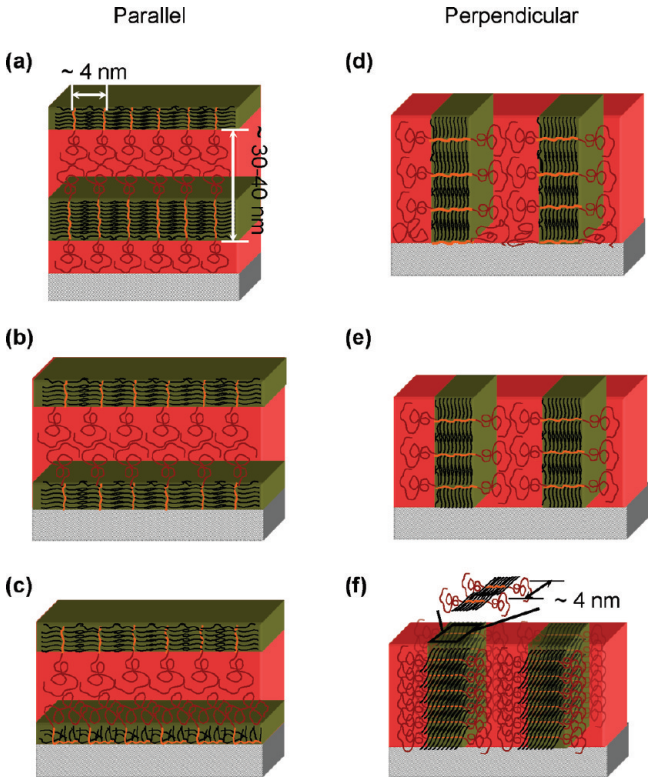

Figure 6. Six possible PS-*b*-P4VP(PDP)$_r$ supramolecular assemblies of lamellar-in-lamellar morphology in thin films that are labeled with "parallel" (a, b and c) and "perpendicular" (d, e and f), respectively. (a and b) Schematics when the PS block and P4VP(PDP)$_r$ block have lower interfacial interactions with the substrate, respectively. (c and d) Scenarios in which the interfacial interactions between the PS block with the substrate is relatively high and low, respectively. In these two cases, the favorable P4VP/substrate interactions pin down the P4VP block onto the surface. (e and f) Orientations of BCP microdomains and the small lamellae from the P4VP(PDP)$_r$ comb blocks when the supramolecules are on SiO_2 and PS, respectively.

the surface. The spatial arrangements of supramolecules at the polymer/substrate interface become complicated due to the architecture of the supramolecule. Two possible scenarios are schematically shown in parts c and d of Figure 6. If the nonfavorable interactions between the PS and the substrate are energetically costly, the P4VP(PDP)$_r$ comb block will arrange as schematically shown in Figure 6c. Such arrangement eliminates the enthalpic penalty associated with the PS/substrate interface. However, it interrupts the ordering of the comb blocks to form small lamellae. There may also be entropic penalty associated with the deformation of the P4VP(PDP)$_r$ comb block. If the interfacial interactions between the PS block with the substrate is relatively low and there are strong favorable intermolecular interactions between small molecules to assemble the comb blocks into lamellae, the BCP lamellar microdomains will be macroscopically oriented normal to the surface as shown in Figure 6d. Parts e and f of Figure 6 show two additional hierarchical assemblies of PS-*b*-P4VP(PDP)$_r$ supramolecules in thin films. Here, the BCP microdomains are oriented normal to the surface, while the small lamellae from the P4VP(PDP)$_r$ comb blocks may be aligned either parallel or perpendicular to the surface as shown in 6e and 6f, respectively.

Thus, the resulting orientation of BCP microdomains reflects a balance among a few energetic contributions including the interfacial interactions of polymer/substrate, the intermolecular interactions of small molecule and the entropy associated with deforming the comb block. Empirically, the volume fraction of the comb block appears to be a critical parameter. Based in Figure 6, however, it is the architecture of the comb block and the spatial distribution of small molecule that are of importance. At $f_{comb} > 0.5$, vertical alignment of BCP microdoamins in thin films can be attributed to two interconnected reasons. One is that with a higher f_{comb}, the supramolecule is more readily to order during the spin-casting process to form vertically aligned framework. At high f_{comb}, it is energetically favorable to form small lamellae of comb block. This favors the formation of hierarchical assembly shown in Figure 6d. The other is that a higher f_{comb} slows down the kinetics of reorientating the BCP microdomain to lay parallel to the surface so that supramolecular assemblies with vertical alignment of BCP microdomain appear to be a long-lived nonequilibrium state.

The strength of surface field, i.e. the differences in the interfacial interactions between each component with the substrate, determines the lifetime of the nonequilibrium state and consequently, experimentally observed supramolecular assemblies in thin films.[35] For films on a SiO_2 substrate, the P4VP strongly interacts with the substrate. Pinning P4VP onto the SiO_2 surface favors vertical alignment of BCP lamellae. The presence of solvent mediates the nonfavorable interactions between PS and PDP and leads to a higher fraction of PDP present in the PS microdomains. There is a trace amount of PDP present in the PS microdomain in the bulk and the presence of solvent further increases the miscibility between PDP and PS.[38,40] This is particularly the case for SP2, SP3, and SP4 with high f_{comb}. The PDP residing in the PS microdomains mediates the interfacial interactions between the PS with the SiO_2 substrate and reduce the driving force to reorient the BCP microdomains to lay parallel to the surface. For thin films on the PS-modified substrate, the GISAXS pattern in Figure 5b clearly shows that the P4VP(PDP)$_r$ comb block is oriented parallel to the surface, forming small lamellae oriented normal to the surface. This reduces repulsive interactions between the P4VP and PS-brush and stabilizes the assembly shown in Figure 6f. We speculate that there may also be PDP concentrated at the interface between the supramolecule thin film and the PS brush to eliminate the P4VP/PS interfaces. Thus, once the supramoleucle assembles with vertically aligned BCP microdomains, the driving force to reorient BCP microdomans is rather small and perpendicular BCP lamellae appear to be a long-lived state.

For supramolecules, the kinetics of the reorientation process is slower for thicker films. This may be due to the fact that there is a finite distance away from the interface or film surface where surface fields have strong influence on the polymer phase behavior. For thin films of PS-*b*-P4VP(PDP)$_r$, as the film thickness increases, there are more free PDPs that are not hydrogen-bonded to 4VP. The system has more freedom to self-adjust the spatial distribution of PDPs. This can be seen from the wider distribution of lamellae of P4VP(PDP)$_r$ comb blocks as a function of azimuthal angle for thicker films. This, in turn, leads to extended lifetime of the vertical alignment of BCP microdomains for the reasons discussed above.

CONCLUSIONS

In summary, we have examined the effects of interfacial interactions and film thickness on macroscopic alignment of

the hierarchical assembly in thin films of BCP-based supramolecules. Consistent with that shown previously, the macroscopic orientation of supramolecular assembly depends on the P4VP-$(PDP)_r$ fraction and can be tailored without interfering with the supramolecular morphologies. Hierarchical assemblies containing BCP microdomains oriented perpendicular to the surface are in a nonequilibrium state. For films with thicknesses higher than $1L_o$, hierarchical assemblies with vertically aligned BCP microdomains can be long-lived metastable state as the volume fraction of the comb block is higher than 0.5. The longevity of the vertically aligned assemblies can be attributed to two reasons. One is the spatial distribution of small molecules that mediates the interactions between each BCP block with the underlying substrate and the other is the comb−coil architecture of the supramolecule.

Present studies investigated various energetic contributions influencing the assembly process in supramolecular thin films and identified parameters governing the supramolecular assemblies in thin films to overcome the bottleneck imposed by interfacial interactions and film thickness to macroscopically align the BCP microdomains normal to the surface. By defining the processing window within which both the BCP microdomains and small molecule orientation can be manipulated, there are numerous opportunities to use thin films of supramolecules for nanopattern templating, nanoparticle assemblies, and fabrication of functional nanodevices.

AUTHOR INFORMATION

Corresponding Author
*E-mail: tingxu@berkeley.edu.

ACKNOWLEDGMENT

This work was supported by the National Science Foundation under contract DMR-1007002, the ACS Petroleum Research Fund (PRF) and by Office of Navel Research Young Investigator Program (ONR-YIP). The Advanced Light Source is supported by the Director, Office of Science, Office of Basic Energy Sciences, of the U.S. Department of Energy under Contract No. DE-AC02-05CH11231. Use of the Advanced Photon Source was supported by the U.S. Department of Energy, Office of Science, Office of Basic Energy Sciences, under Contract No. DE-AC02-06CH11357.

REFERENCES

(1) Spontak, R. J.; Shankar, R.; Bowman, M. K.; Krishnan, A. S.; Hamersky, M. W.; Samseth, J.; Bockstaller, M. R.; Rasmussen, K. O. *Nano Lett.* **2006**, *6* (9), 2115–2120.

(2) van Zoelen, W.; ten Brinke, G. *Soft Matter* **2009**, *5* (8), 1568–1582.

(3) Mann, S. *Nat. Mater.* **2009**, *8* (10), 781–792.

(4) Henselwood, F.; Liu, G. J. *Macromolecules* **1997**, *30* (3), 488–493.

(5) Ruokolainen, J.; Makinen, R.; Torkkeli, M.; Makela, T.; Serimaa, R.; ten Brinke, G.; Ikkala, O. *Science* **1998**, *280* (5363), 557–560.

(6) Maki-Ontto, R.; de Moel, K.; Polushkin, E.; van Ekenstein, G. A.; ten Brinke, G.; Ikkala, O. *Adv. Mater.* **2002**, *14* (5), 357–361.

(7) Chao, C. Y.; Li, X. F.; Ober, C. K.; Osuji, C.; Thomas, E. L. *Adv. Funct. Mater.* **2004**, *14* (4), 364–370.

(8) Valkama, S.; Kosonen, H.; Ruokolainen, J.; Haatainen, T.; Torkkeli, M.; Serimaa, R.; Ten Brinke, G.; Ikkala, O. *Nat. Mater.* **2004**, *3* (12), 872–876.

(9) Li, C. Y.; Tenneti, K. K.; Zhang, D.; Zhang, H. L.; Wan, X. H.; Chen, E. Q.; Zhou, Q. F.; Carlos, A. O.; Igos, S.; Hsiao, B. S. *Macromolecules* **2004**, *37* (8), 2854–2860.

(10) Morikawa, Y.; Nagano, S.; Watanabe, K.; Kamata, K.; Iyoda, Y.; Seki, T. *Adv. Mater.* **2006**, *18* (7), 883–886.

(11) Korhonen, J. T.; Verho, T.; Rannou, P.; Ikkala, O. *Macromolecules* **2010**, *43* (3), 1507–1514.

(12) Rancatore, B. J.; Mauldin, C. E.; Tung, S. H.; Wang, C.; Hexemer, A.; Strzalka, J.; Frechet, J. M. J.; Xu, T. *ACS Nano* **2010**, *4* (5), 2721–2729.

(13) Ruokolainen, J.; Saariaho, M.; Ikkala, O.; ten Brinke, G.; Thomas, E. L.; Torkkeli, M.; Serimaa, R. *Macromolecules* **1999**, *32* (4), 1152–1158.

(14) Ruokolainen, J.; ten Brinke, G.; Ikkala, O. *Adv. Mater.* **1999**, *11* (9), 777–780.

(15) Ikkala, O.; ten Brinke, G. *Science* **2002**, *295* (5564), 2407–2409.

(16) Ikkala, O.; ten Brinke, G. *Chem. Commun.* **2004**, *19*, 2131–2137.

(17) Zheng, W. Y.; Hammond, P. T. *Macromolecules* **1998**, *31* (3), 711–721.

(18) Valkama, S.; Ruotsalainen, T.; Nykanen, A.; Laiho, A.; Kosonen, H.; ten Brinke, G.; Ikkala, O.; Ruokolainen, J. *Macromolecules* **2006**, *39* (26), 9327–9336.

(19) Verploegen, E.; McAfee, L. C.; Tian, L.; Verploegen, D.; Hammond, P. T. *Macromolecules* **2007**, *40* (4), 777–780.

(20) Chuang, W. T.; Sheu, H. S.; Jeng, U. S.; Wu, H. H.; Hong, P. D.; Lee, J. J. *Chem. Mater.* **2009**, *21* (6), 975–978.

(21) Zhao, Y.; Thorkelsson, K.; Mastroianni, A. J.; Schilling, T.; Luther, J. M.; Rancatore, B. J.; Matsunaga, K.; Jinnai, H.; Wu, Y.; Poulsen, D.; Frechet, J. M. J.; Paul Alivisatos, A.; Xu, T. *Nat. Mater.* **2009**, *8* (12), 979–985.

(22) Hasegawa, H.; Hashimoto, T. *Macromolecules* **1985**, *18* (3), 589.

(23) Henkee, C. S.; Thomas, E. L.; Fetters, L. J. *J. Mater. Sci.* **1988**, *23* (5), 1685–1694.

(24) Anastasiadis, S. H.; Russell, T. P.; Satija, S. K.; Majkrzak, C. F. *Phys. Rev. Lett.* **1989**, *62* (16), 1852.

(25) Karim, A.; Singh, N.; Sikka, M.; Bates, F. S. *J. Chem. Phys.* **1994**, *100*, 1620.

(26) Morkved, T. L.; Lu, M.; Urbas, A. M.; Ehrichs, E. E.; Jaeger, H. M.; Mansky, P.; Russell, T. P. *Science* **1996**, *273* (5277), 931–933.

(27) Huang, E.; Rockford, L.; Russell, T. P.; Hawker, C. J. *Nature* **1998**, *395*, 757.

(28) Thurn-Albrecht, T.; DeRouchey, J.; Russell, T. P.; Jaeger, H. M. *Macromolecules* **2000**, *33*, 3250–3253.

(29) Segalman, R. A.; Yokoyama, H.; Kramer, E. J. *Adv. Mater.* **2001**, *13* (15), 1152–1155.

(30) Kim, S. H.; Misner, M. J.; Xu, T.; Kimura, M.; Russell, T. P. *Adv. Mater.* **2004**, *16* (3), 226–231.

(31) Angelescu, D. E.; Waller, J. H.; Register, R. A.; Chaikin, P. M. *Adv. Mater.* **2005**, *17* (15), 1878–1881.

(32) Verploegen, E.; Boone, D.; Hammond, P. T. *J. Polym. Sci., Part B: Polym. Phys.* **2007**, *45* (24), 3263–3266.

(33) Fredrickson, G. H. *Macromolecules* **1987**, *20* (10), 2535–2542.

(34) Lambooy, P.; Russell, T. P.; Kellogg, G. J.; Mayes, A. M.; Gallagher, P. D.; Satija, S. K. *Phys. Rev. Lett.* **1994**, *72* (18), 2899.

(35) Mansky, P.; Russell, T. P.; Hawker, C. J.; Mays, J.; Cook, D. C.; Satija, S. K. *Phys. Rev. Lett.* **1997**, *79* (2), 237–240.

(36) Xu, T.; Hawker, C. J.; Russell, T. P. *Macromolecules* **2005**, *38* (7), 2802–2805.

(37) Lu, Q.; Bazuin, C. G. *Nano Lett.* **2005**, *5* (7), 1309–1314.

(38) van Zoelen, W.; Asumaa, T.; Ruokolainen, J.; Ikkala, O.; ten Brinke, G. *Macromolecules* **2008**, *41* (9), 3199–3208.

(39) van Zoelen, W.; Polushkin, E.; ten Brinke, G. *Macromolecules* **2008**, *41* (22), 8807–8814.

(40) Tung, S. H.; Kalarickal, N. C.; Mays, J. W.; Xu, T. *Macromolecules* **2008**, *41* (17), 6453–6462.

(41) Tung, S. H.; Xu, T. *Macromolecules* **2009**, *42* (15), 5761–5765.

(42) Nandan, B.; Vyas, M. K.; Bohme, M.; Stamm, M. *Macromolecules* **2010**, *43* (5), 2463–2473.
(43) Knoll, A.; Horvat, A.; Lyakhova, K. S.; Krausch, G.; Sevink, G. J. A.; Zvelindovsky, A. V. *Phys. Rev. Lett.* **2002**, *89* (3), 035501.
(44) van Zoelen, W.; Vlooswijk, A. H. G.; Ferri, A.; Andringa, A. M.; Noheda, B.; ten Brinke, G. *Chem. Mater.* **2009**, *21* (19), 4719–4723.
(45) Sidorenko, A.; Tokarev, I.; Minko, S.; Stamm, M. *J. Am. Chem. Soc.* **2003**, *125* (40), 12211–12216.
(46) Tokarev, I.; Krenek, R.; Burkov, Y.; Schmeisser, D.; Sidorenko, A.; Minko, S.; Stamm, M. *Macromolecules* **2005**, *38* (2), 507–516.
(47) Morikawa, Y.; Nagano, S.; Watanabe, K.; Kamata, K.; Iyoda, T.; Seki, T. *Adv. Mater.* **2006**, *18*, 883–886.
(48) Nandan, B.; Gowd, E. B.; Bigall, N. C.; Eychmuller, A.; Formanek, P.; Simon, P.; Stamm, M. *Adv. Funct. Mater.* **2009**, *19* (17), 2805–2811.
(49) Kuila, B. K.; Gowd, E. B.; Stamm, M. *Macromolecules* **2010**, *43* (18), 7713–7721.
(50) Ludwigs, S.; Boker, A.; Voronov, A.; Rehse, N.; Magerle, R.; Krausch, G. *Nat. Mater.* **2003**, *2* (11), 744–747.